First Results of Superconducting RF (SRF) Cavity Fabrication by Electrohydraulic Forming

E. Cantergiani[1*], G. Avrillaud[1], C. Abajo Clemente[2], S. Atieh[2], G. Favre[2], J. Deroy[1], F. Raveleau[1]

[1] Bmax, Z.I; Thibaud 30 Bd de Thibaud, 31104 Toulouse, France
[2] CERN, CH-1211, Geneva 23, Switzerland
*Corresponding author. Email: Elisa.cantergiani@bmax.com, Phone: +33534611660

Abstract

In the framework of many accelerator projects relying on RF superconducting technology, shape conformity and processing time are key aspects for the optimization of copper and niobium cavities fabrication. An alternative technique to traditional shaping methods, such as deep-drawing and spinning is electrohydraulic forming (EHF). In EHF, half-cells are obtained through ultrahigh-speed deformation of blank sheets by using shockwaves induced in water by a pulsed electrical discharge. Compared to traditional shaping methods, EHF can bring valuable results in terms of final shape precision, reduced springback and high repeatability. In this paper, the first results of EHF on copper and niobium prototypes are discussed. The simulations performed to reproduce the embedded multi-physics phenomena and to optimize process parameters are also presented.

Keywords

Electrohydraulic Forming, SRF Cavities, Material Characterization

Introduction

Electrohydraulic formed cavities are of interest for several SRF applications at CERN. These cavities are used to accelerate particles. A frequency of 400 MHz is used for the large hadron collider (LHC) and electro-hydraulic forming (EHF) is explored for the production of copper spare cavities. EHF technology is currently explored for the

fabrication of bulk niobium 700-800 MHz half-cells in the frame of the future circular collider (FCC) project (Cantergiani et al., 2016). Traditionally, superconducting radio frequency (SRF) cavities are fabricated by electron-beam welding of half-cells obtained through sheet metal forming techniques such as deep-drawing and spinning (Atieh, Amorim Carvalho, et al., 2015). A schematic view of a complete sequence of SRF cavities is shown in *Figure 1 (a),* while *Figure 1 (b)* defines the two main zones of a half-cell, named iris and equator and *Figure 1 (c)* shows that two half-cells are beam welded to form a full cavity. The metals used for the production of these half-cells include oxygen free electronic (OFE) copper or high purity niobium.

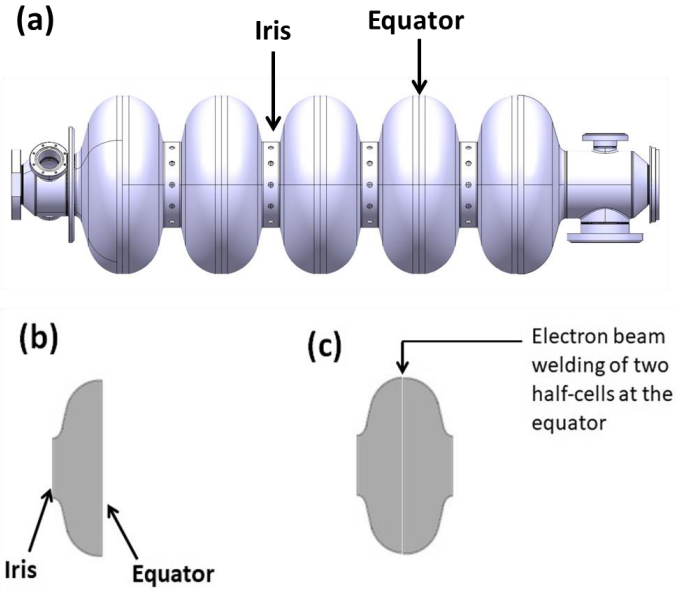

Figure 1: *(a) Schematic view of a sequence of SRF cavities used for particle accelerators; (b) schematic view of a half-cell; (c) electron beam welding of two half-cells at the equator to form a full cavity;*

The traditional shaping methods such as deep-drawing and spinning show several drawbacks; in particular, deep drawing cannot produce complex shapes with high accuracy and for large half-cells it would require high-tonnage hydraulic presses (Padamsee, Knobloch, and Hays, 2008). According to the experience reported by other researchers, deep-drawing is prone to springback, which can cause significant deviations from the final geometry (Marhauser, 2011). Furthermore, deep-drawing requires a coning step to accurately obtain the curvature at the iris and this technique is highly affected by springback. Thus, for large components (such as 400 MHz half-cells), spinning is

preferred. However, spinning presents some disadvantages given that it sometimes requires several forming steps including intermediate annealing to avoid necking of the metallic sheet. Moreover, spinning of a half-cell requires optimization of many parameters including feed ratio, roller path and roller ratio (Wong, Dean, and Lin, 2003). More recently, full cavities without weld at the equator were obtained through hydroforming (Singer, Singer, Jelezov, and Kneisel, 2015) nonetheless; this technology requires the optimization of many parameters, including the starting diameter of the tube. Additionally, hydroforming can only accurately form the outer surface of the cell, while the precision of the internal RF surface is strongly dependent on the thickness and tolerance of the starting tube. Furthermore, deep-drawing, spinning and hydroforming leave 100-200 μm of a surface damaged layer which needs to be removed by buffered chemical polishing to improve RF performances.

All these drawbacks associated with traditional forming technique can be overcome or limited by high strain-rate forming processes such as electrohydraulic forming (EHF). This technology can limit or avoid completely springback and it can increase the formability of metals making it possible to avoid intermediates annealings. These advantages are due to the viscoplastic behaviour of metals which is activated in the range of high strain-rates encountered in EHF. Another important advantage of EHF is the level of fine details and sharp angles that can be obtained. From an industrial point of view, EHF is very attractive to reduce fabrication time and cost of half-cells.

In this paper the results of EHF of 400 MHz OFE copper half-cells and of 700 MHz niobium half-cells are presented and discussed.

Electrohydraulic Forming Description

Bmax develops electrohydraulic forming systems. The key to the technology is the discharge of high voltage capacitors in water. A system consists of a control cabinet; a bank of capacitors and a chamber where the high-speed forming of the metallic blank takes place *(Figure 2).*

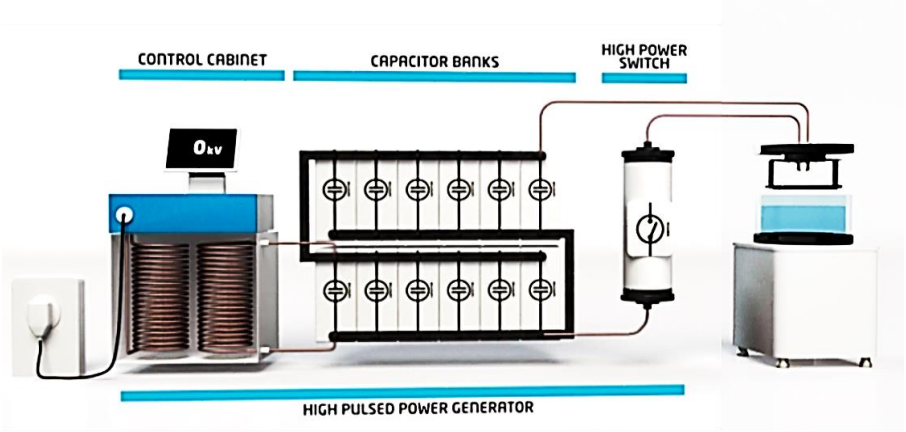

Figure 2: *Electrohydraulic forming set-up*

The electrical discharge occurs between two electrodes placed inside the discharge chamber, which is filled with water, while a vacuum is created between the die and the metallic blank to avoid the formation of defects during forming (*Figure 3*). When the switch of the circuit is closed, the electrical energy stored in the capacitors is released between the electrodes and a nonthermal plasma is produced. This plasma creates a fast bubble expansion producing a shock wave propagating inside the water chamber and impacting the metallic blank to be formed. Depending on the released energy, impact velocity can range from 50 m/s up to 200 m/s causing the material to be formed at strain rates in the order of 10^3-10^4 s^{-1}. This level of strain-rate is able to activate a viscoplastic behaviour in the material. The high strain-rate results in an increase in formability due to a more uniform dislocation distribution delaying or preventing the formation of dislocation cells and necking (Gray III, 2012).

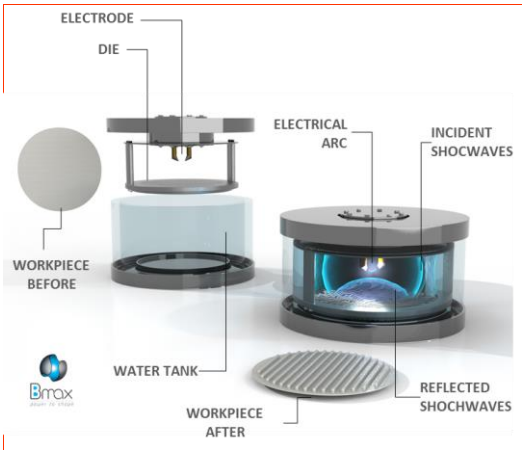

Figure 3: *Schematic view of components for an electrohydraulic forming chamber*

Electrohydraulic Forming Simulations

Several parameters need to be optimized in order to produce successfully SRF half-cells. Some parameters are related to the geometry of the system, such as volume of the discharge chamber, force applied on the blank holder and the starting thickness and dimensions of the metallic sheet. Other parameters concern the electrohydraulic forming process and they include the input energy stored in the capacitor, the number of pulses, the duration of each pulse and the position and number of electrodes. Indeed, Bmax has developed a model capable of predicting the electrical power delivered in the arc during the discharge as function of inductance, capacitance, resistance and voltage of the generator, as well as distance between electrodes. The predicted electrical power is used as input in LS-DYNA simulations to optimize the number and the duration of the forming pulses. Mechanical properties of the metal to be formed are important for LS-DYNA simulations, especially considering that for some metals, the yield stress, the strain-hardening or both can be strain-rate dependent (Follansbee and Weertman, 1982).

Characterization of Mechanical Properties of OFE Copper and Niobium

Mechanical properties represent a very important input for LS-DYNA simulations to predict thinning of the final component and to predict the formability of the metal. OFE copper and niobium are tested both in quasi-static and dynamic conditions. The

mechanical properties at low strain-rates (10^{-3} s^{-1}) are obtained through uniaxial tensile tests at room temperature. *Table 1* summarizes the average values found for high purity niobium (residual resistivity ratio RRR higher than 300) supplied by Ningxia and for OFE copper after annealing at 600 °C for 2 hours in high vacuum. Tensile specimens are cut both along rolling direction and transversal direction.

Material	Annealed OFE Copper	Niobium
Yield Stress [MPa]	51±0.5	67±5
Ultimate Tensile Strength [MPa]	224±3.2	171±1.5
Strain-Hardening Exponent (n)	0.35	0.31
Strain at Fracture (%)	52±3	46±3

Table 1: *Mechanical Properties of OFE copper and niobium at low strain-rate (10^{-4} s^{-1}) obtained through uniaxial tensile test*

As mentioned, EHF involves strain-rates around 10^3 s^{-1}, thus, it is important to understand how mechanical properties of niobium and OFE copper evolve at this high speed of forming. In order to determine the constitutive behaviour of materials at such a high strain-rate, Bmax has developed a set-up based on electromagnetic free expansion of a metallic tube or sheet (Jeanson et al., 2014). This approach is derived from the ring expansion test described in literature (Gourdin, 1989), (Daehn et al., 2008). The high-velocity expansion of the specimen is obtained through the action of Lorentz forces obtained by the interaction of a magnetic field produced by a coil and the electrical current induced in the specimen to be tested (as described in detail by Jeanson et al., 2014). During the test, the speed of deformation is measured by using a photon Doppler velocimeter (PDV). When the experimental speed of deformation has been obtained, theoretical simulations of electromagnetic expansion test are performed by using the commercial software LS-DYNA. The purpose of these simulations is to optimize the material parameters of the material constitutive behaviour to fit the experimental speed of deformation. The iterative procedure is performed by using the commercial tool LS-Opt. An example of fitting of an expansion velocity curve is shown in *Figure 4*.

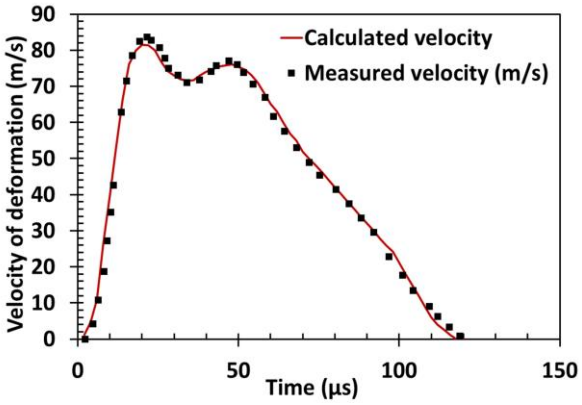

Figure 4: *Measured and Simulated expansion velocity curves for a tube expansion test (*Cantergiani E. et al., 2016)

The mechanical properties of materials at high-strain rates are described by constitutive laws which are strain-rate dependent, such as the Johnson-Cook law (Johnson, Cook, 1983) or the Zerilli-Armstrong law (Zerilli and Armstrong, 1987). Johnson-Cook is an empirical model often implemented in most commercial finite element software and it is reported in equation 1.

$$\sigma = \left(A + B\varepsilon^{n}\right)\cdot\left(1 + C\ln\left(\frac{\dot{\varepsilon}}{\dot{\varepsilon}_0}\right)\right)\cdot\left(1 - \frac{T - T_0}{T_{melt} - T_0}\right)^{m} \quad (1)$$

where, A is the yield stress of the material in quasi-static conditions, while B and n are the strain-hardening parameters at low strain-rate. C represents the strain-rate sensitivity coefficient; $\dot{\varepsilon}$ is the effective plastic strain-rate, while $\dot{\varepsilon}_0$ is a reference strain-rate set to 1. Finally, the last part of the equation describes the dependence of mechanical properties on the temperature, m is the thermal softening coefficient, while T_0 is the room temperature, T_{melt} is the melting temperature and T is the material temperature. During the identification process, the values of A, B, C, n and m are found.

The Johnson-Cook model is a multiplicative model where the effects of plastic strain, strain-rate and temperature are uncoupled, thus, sometimes it is not the appropriate model to describe the influence of strain-rate on work-hardening. Furthermore, it does not take into account crystallographic differences between metals. Thus, especially for body centred cubic (bcc) metals (such as niobium), the Zerilli-Armstrong model is preferred since it was obtained on the basis of the mechanical dislocations theory, thus it allows two different expressions for bcc and face centred cubic (fcc) metals (such as copper).

From the high-speed characterization performed at Bmax it was shown that niobium has a high sensitivity to strain-rate, while copper still shows an influence on strain-rate but less pronounced than niobium. *Figure 5* shows a comparison of the true stress-strain curve obtained for copper in static and dynamic condition. These curves are then used as input for material behaviour in the LS-DYNA EHF forming simulations.

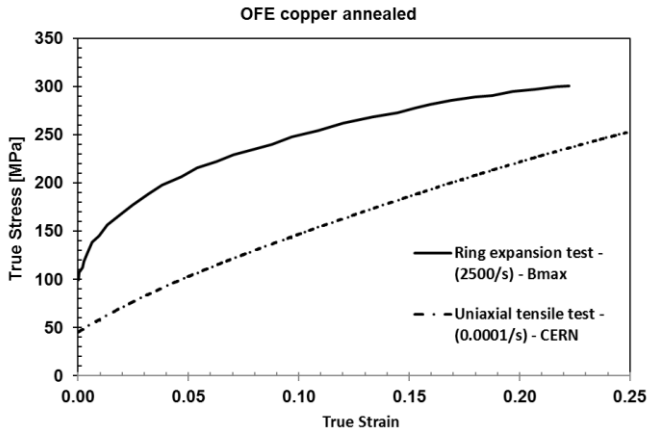

Figure 5: *Comparison of true stress-strain curve obtained at low strain rate (10^{-4} s^{-1}) and at high strain-rate (10^{3} s^{-1}) for annealed OFE Copper*

Numerical Simulations of EHF Half-Cells

EHF uses the pressure waves generated in water by a high, fast pulse of current discharged between two electrodes, or through a copper wire connecting the two electrodes in water. At Bmax, half-cells were formed both by performing the discharge through a copper wire or by using electrodes. The evolution of the electrical power as function of time is calculated from the parameters of the high voltage generator and it is used as input in the forming simulations. This electrical current is used to generate pressure waves inside an Eulerian mesh representing the volume of water, while the metallic sheet to be formed is represented by a Lagrangian mesh. At each time step, the two meshes are coupled so that the pressure generated in the water is transferred as a force on the sheet to be formed. At the end of the simulation, the deformed sheet with its residual stress-strain distribution is used as a starting blank to simulate the next forming shot. An example of a simulated forming shot for a 400 MHz half-cell is shown in *Figure 6*, where the evolution of pressure is shown, while *Figure 7* shows the set-up used to produce 400 MHz and 700-800 MHz

half-cells. In *Figure 8 (a)* the forming of a 400 MHz is shown, while *Figure 8 (b) and (c)* show 700 MHz half-cells obtained through electrohydraulic forming.

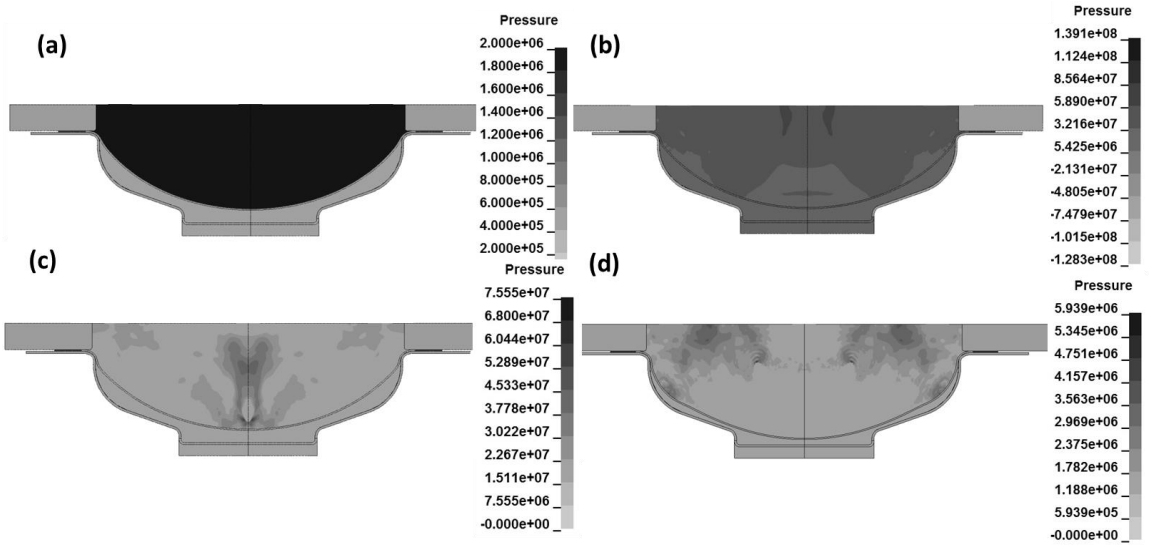

Figure 6: *2D-axisymmetric EHF simulations of a 400 MHz copper cavity showing the evolution of pressure (Pa) inside the discharge chamber during one forming shot: (a) time zero starting of the electric discharge; (b) after 200 µs; (c) after 300 µs, (d) after 900 µs*

Provided that proper material models are used as input, simulations are fundamental to optimize several process parameters such as: pressure to be applied on the blank holder and gap between the sheet and the blank holder to optimize the draw-in of the sheet and reduce thinning at the iris.

Figure 7: *Set-up used at Bmax for the forming of 400 MHz and 700-800 MHz half-cells*

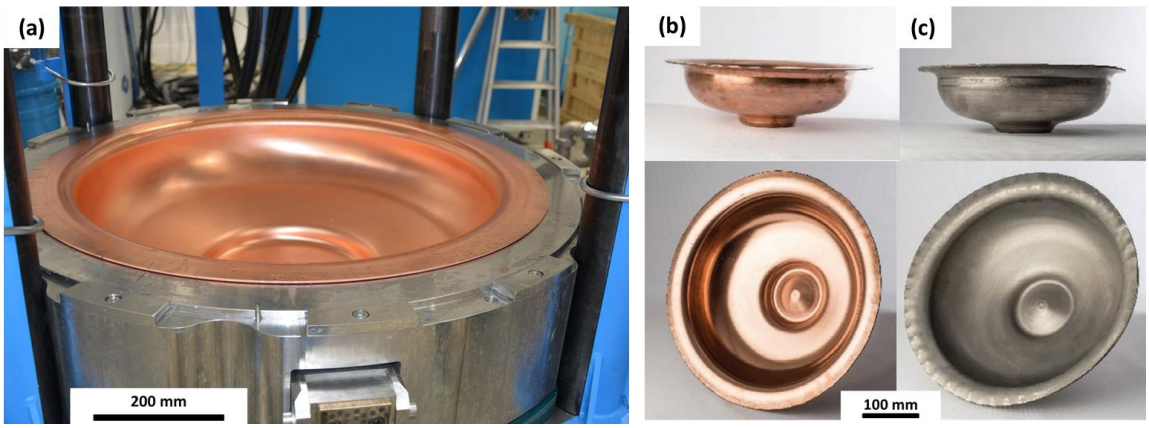

Figure 8: *(a) forming of a 400 MHz OFE copper half-cell; (b) 700 MHz OFE copper half-cell and (c) 700 MHz niobium half-cell obtained through electrohydraulic forming*

In addition, numerical simulations are helpful to optimize the number and distribution of electrodes used for the discharge and the number of forming pulses and energy of each pulse. Moreover, through simulations, the geometry and the volume of the discharge chamber can be properly designed. Indeed, two thirds of the forming effect comes from reflected waves.

Results of EHF Half-Cells

Shape accuracy of 400 MHz copper half-cells

The shape accuracy of 400 MHz half-cells formed by EHF was compared at CERN with the shape accuracy of 400 MHz half cells obtained by spinning and successive machining (Clemente C.A. et al., 2017). The steps required for the forming of half-cells by spinning followed by machining is currently under optimization at CERN. Up to now, half-cells formed by spinning were obtained starting with a blank of 4 mm in order to have enough material for the final machining step to achieve the required inner shape. The half-cell went through one intermediate annealing step during the spinning phase. At the end of spinning; the surface of the half-cell was machined to obtain the tight tolerances required on the final geometry.

EHF was performed on copper sheets of 3 mm thickness without any intermediate annealing and any successive machining. The results obtained by geometry control are shown in *Table 2* and the roughness values are shown in *Table 3*.

From the values, it is evident that EHF gives results which are in agreement with the precision required for the half-cells. EHF is more precise than spinning, and moreover it does not require any machining of the half-cell surfaces after forming. Moreover, as shown in *Table 3* the value of roughness before and after EHF is preserved both for copper and niobium half-cells. The thickness of the final formed 400 MHz half-cell was extracted for both EHF and spinning and it is shown in *Figure 9*.

Shape Accuracy	Required Dimensions	EHF	Spinning and Machining
Diameter at the Equator [mm]	688 ± 0.3	687.64	687.81
Circularity at the equator [mm]	0.1	0.03	0.63
Thickness at the Equator [mm]	2.3 min 3.0 max	2.99 ± 0.02	2.30 ± 0.14
Diameter at the Iris [mm]	300 ± 0.2	299.91	300.02
Circularity at the iris [mm]	0.1	0.08	0.77
Thickness at the Iris [mm]	2.3 min 3.0 max	2.05 ± 0.05	2.35 ± 0.07

Table 2: *Shape accuracy at iris and equator for 400 MHz copper half cells formed by EHF and spinning followed by machining*

Half-cell	R_a sheet before EHF [µm]	R_a sheet before Spinning + Machining [µm]	R_a sheet after EHF [µm]	R_a sheet after Spinning + Machining [µm]
400 MHz copper	0.17	0.25	0.48	0.76
700 MHz copper	0.2	-	0.2	-
700 MHz niobium	0.8-0.9	-	0.9-1	-

Table 3: *Value of surface roughness measured for 400 MHz copper half-cells and for 700 MHz niobium and copper half-cells*

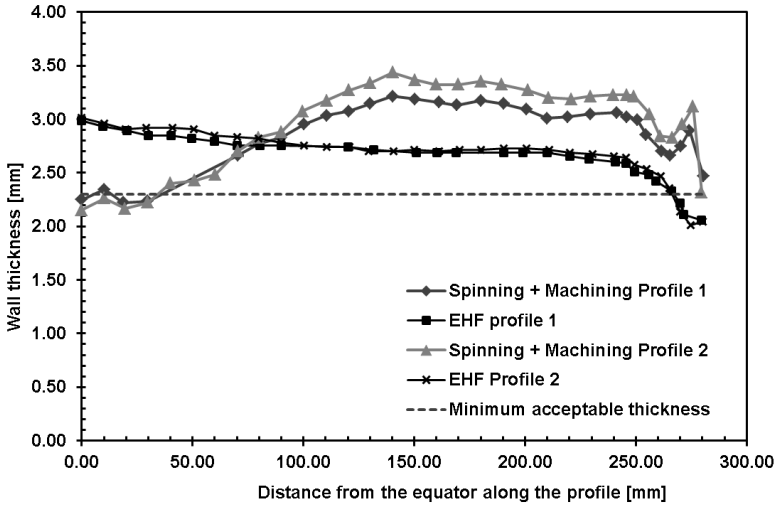

Figure 9: *Thickness distribution for 400 MHz copper half-cells obtained through EHF or through spinning followed by machining (at least two measurements, profile 1 and profile 2, were taken on each half-cell)*

As shown in *Figure 9*, the thickness distribution found for EHF is homogeneous on the whole profile, the iris zone is slightly below the minimum thickness of 2.3 mm, while the remainder of the profile is between 3 mm and 2.3 mm as required by the specifications. The thickness distribution obtained from spinning and successive machining shows higher variability. Moreover at the equator the thickness is slightly below 2.3 mm and for the most part of the profile, the thickness is higher than 3 mm which can result in difficulties when the half-cell needs shape deformation to obtain proper RF response. The yield strength of copper after forming was compared for a half-cell formed by electrohydraulic forming and for a half-cell formed by spinning (*Table 4*). The thinner iris thickness obtained by EHF can still be accepted because of the high yield stress of the material after forming. On the contrary, spinning shows a low yield stress at the iris due to the heat treatments which are performed during the forming procedure and which cause recovery of the material.

Mechanical Properties after forming	Spinning + Machining	EHF
Yield strength at the iris [MPa]	47	252
Yield strength at the equator [MPa]	248	225

Table 4: *Yield strength values measured on half-cells obtained by EHF or by spinning followed by machining*

Conclusions

This paper has presented the procedure used for electrohydraulic forming of half-cells. The procedure used to simulate the process was described. EHF and spinning were compared in terms of shape accuracy for 400 MHz half-cells used for the Large Hadron Collider (LHC) and the results have shown that EHF can produce acceptable half-cells with a process that is faster and cheaper than spinning since it does not require intermediate annealing and the forming shots only last a few microseconds. Further development and improvement of EHF process is on-going in order to obtain a thickness at the iris not lower than 2.3 mm.

References

Marhauser F. (2011). JLAB SRF Cavity Fabrication Errors, Consequences and Lessons Learned. *IPAC11 Conference.* Spain.

Atieh S., Amorim Carvalho A., et al. (2015). First Results of SRF Cavity Fabrication by Electro-Hydraulic Forming at CERN. *Proceedings of SRF2015*, (pp. 1-7). Whistler, BC, Canada.

Cantergiani E. et al. (2016). Niobium superconducting rf cavity fabrication by electrohydraulic forming. *Physical Review Accelerators and Beams, 19*(114703), 1-13.

Clemente C.A. et al. (2017, Mai 30). FCC Week 2017. *First Results of large size SRF cavity fabrication by electrohydraulic forming*. Berlin, Germany.

Daehn G.S. et al. (2008). Coupling Experiment and Simulation in Electromagnetic Forming using Photon Doppler Velocimetry. *3rd International Conference on High Speed Forming.* Germany.

Follansbee P. and Weertman J. (1982). On the question of flow stress at high strain rates controlled by dislocation viscous flow. *Mech. Mater., 1*, 345.

Gourdin W. (1989). Analysis and Assessment of Electromagnetic Ring Expansion as a High-strain-rate Test. *Journal of Applied Physics, 65*(2), 411-422.

Gray III G.T. (2012). High strain-rate deformation: Mechanical behavior and deformation substructures induced. *Annu. Rev. Mater. Res., 42*, 285.

Jeanson A.C. et al. (2014). Identification of Material Constitutive Parameters for Dynamic Applications: Magnetic Pulse Forming (MPF) and Electrohydraulic Forming (EHF). *Proceedings of 5th International Conference on HIgh Speed Forming.*

Johnson G.R., Cook W. H. (1983). A Constitutive Model and Data for Metals Subjected to Large Strains, High Strain Rates and High Temperatures. *7th International Symposium on Ballistics,* (pp. 514-546).

Padamsee H., Knobloch J., and Hays T. (2008). *RF Superconductivity for Accelerators.* Weinheim, Germany: Wiley-VCH.

Singer W., Singer X., Jelezov I., and Kneisel P. (2015). Hydroforming of elliptical cavities. *Phys. Rev. ST Accel. Beams, 18*, 022001.

Wong C.C., Dean T.A., and Lin J. (2003). A review of spinning, shear forming and flow forming processes. *Int. J. Machine Tools Manufacture, 43*, 1419.

Zerilli F.J. and Armstrong R.W. (1987). Dislocation-mechanics-based constitutive relations for material dynamics calculations. *J. Appl. Phys., 61,* 1816.